Characterization of Glial Populations in the Aging and Remyelinating Mouse Corpus Callosum

Yoshie Kawabe, Tatsuhide Tanaka, Ayami Isonishi, Kazuki Nakahara, Kouko Tatsumi, Akio Wanaka

Department of Anatomy and Neuroscience, Nara Medical University Faculty of Medicine

840 Shijo-cho, Kashihara City, Nara 634-8521, Japan

Correspondence: Kouko Tatsumi, Ph.D. radha815@naramed-u.ac.jp

Keywords: Corpus callosum, oligodendrocyte, microglia, astrocyte, remyelination

Abbreviations:

MBP	Myelin basic protein
OL	Oligodendrocyte
OPC	Oligodendrocyte precursor cell
PM-OL	Premyelinating Oligodendrocyte
M-OL	Mature Oligodendrocyte
AS	Astrocyte
MG	Microglia
LA	Linear Array
IC	Isolated Cell

Abstract

Cells in the white matter of the adult brain have a characteristic distribution pattern in which several cells are contiguously connected to each other, making a linear array (LA) resembling pearls-on-a-string parallel to the axon axis. We have been interested in how this pattern of cell distribution changes during aging and remyelination after demyelination. In the present study, with a multiplex staining method, semi-quantitative analysis of the localization of oligodendrocyte lineage cells (oligodendrocyte progenitors, premyelinating oligodendrocytes, and mature oligodendrocytes), astrocytes, and microglia in 8-week-old (young adult) and 32-week-old (aged) corpus callosum showed that young adult cells still include immature oligodendrocytes and that LAs contain a higher proportion of microglia than isolated cells. In aged mice, premyelinating oligodendrocytes were decreased, but microglia continued to be present in the LAs. These results suggest that the presence of microglia is important for the characteristic cell localization pattern of LAs. In a cuprizone-induced demyelination model, we observed re-formation of LAs after completion of cuprizone treatment, concurrent with remyelination. These re-formed LAs again contained more microglia than the isolated cells. This finding supports the hypothesis that microglia contribute to the formation and maintenance of LAs. In addition, regardless of the distribution of cells (LAs or isolated cells), astrocytes were found to be more abundant than in the normal corpus callosum at 24 weeks after cuprizone treatment when remyelination is completed. This suggests that astrocytes are involved in maintaining the functions of remyelinated white matter (239 words).

Introduction

The corpus callosum is one of the largest white matter structures in the brain. It contains numerous myelinated and non-myelinated axons, and plays a major role in information transmission between cortical hemispheres and subcortical brain regions [1–3]. Myelin is formed by mature oligodendrocytes, and astrocytes [4–7] and microglia [7–9] are also present in the corpus callosum in addition to oligodendrocytes, although in smaller numbers. The developing white matter also contains cells of the oligodendrocyte lineage (oligodendrocyte progenitors (OPCs) and premyelinating oligodendrocytes), which are known to interact with each other for functional development [10–14]. These heterogeneous cellular populations complicate the level of interactions. Such diverse glial interactions have been analyzed primarily using cell culture systems and genetically engineered mice; therefore, simultaneous observation of the localization of multiple types of glia in actual corpus callosum tissue should provide useful information for considering the functional relevance of such interactions. However, multiple staining of cell-specific markers is usually limited to three or four markers, and simultaneous visualization of more markers is technically difficult.

To circumvent this difficulty, we employed a relatively new technique called multiplex staining that can label more than five cell markers [15, 16] and successfully localized and analyzed the cell population in the corpus callosum using seven cell-specific markers. The sequential immunostaining visualized the expression of multiple proteins in each cell without losing cell location information. Taking advantage of this procedure, we focused our analyses on the characteristic cell distribution patterns in white matter. At birth, cells in the corpus callosum were randomly dispersed. Then, within two weeks, groups of cells became tightly adjacent to each other and created linear pearls-on-a-string arrays parallel to the axon axis. This distributional change occurs in accordance with myelination, implying that this locational transformation of glial cells may play an important role in myelination and/or maintenance of the myelin sheath, presumably mediated by interactions between adjacent cell bodies. Most of the cells comprising the LAs are thought to be mature oligodendrocytes (called

interfascicular oligodendrocytes) [17, 18]. We previously examined the detailed 3D structures of the oligodendrocytes that form a LA and found that the oligodendrocytes myelinate distant axons with specific ranges of diameters [19]. The mechanisms underlying the formation and the functional implications of LAs still remain elusive.

To gain an insight into these issues, we defined two subpopulations, LAs and isolated cells, in the corpus callosum and compared the glial heterogeneities in these subpopulations. We further extended this analysis to the corpus callosum of adult mice, in which remyelination takes place after 4-week cuprizone treatment [20–23]. By examining healthy corpus callosum and cuprizone-induced demyelination-remyelination model, we demonstrated the heterogeneity of glial cells and the close relationship of the LAs with myelination. Understanding more about the mechanism and function of LAs may reveal how to promote myelination, which may in turn lead to future novel therapeutic perspectives for demyelinating diseases such as multiple sclerosis and leukodystrophy.

Materials and Methods

Animals

The protocols for the animal experiments were approved by the Animal Care Committee of Nara Medical University and were performed in accordance with the policies established in the National Institutes of Health Guide for the Care and Use of Laboratory Animals. Eight-week-old female C57BL/6J mice were housed under a 12-h light/dark cycle in a temperature-controlled room. Food and water were available *ad libitum*. To characterize developmental changes of the corpus callosum, postnatal day 7 (P7), postnatal day 14 (P14), and postnatal week 8 (young adult) mice were used. To compare the glial heterogeneity in postnatal development, young adult and aged normal mice were analyzed at 8 and 32 weeks of age, respectively.

Cuprizone Treatment

Demyelination was induced by feeding 8-week-old mice a diet containing 0.2% cuprizone (oxalic acid bis(cyclohexylidene hydrazide)) mixed in ground rodent chow. Cuprizone feeding was maintained for 4 weeks, after which the mice were put on a normal chow to induce remyelination. Mice were sacrificed at 1 (+1w), 4 (+4w), 10 (+10w), and 24 (+24w) weeks after cuprizone removal. Three or four animals were investigated in each group.

Tissue Preparation

Animals were perfused intracardially with 4% paraformaldehyde. The brain was removed from the cranium, post-fixed in 4% paraformaldehyde, and embedded in paraffin. Coronal sections (2 μm) were cut with a microtome, mounted on charged glass slides, and dried overnight at 40°C. We set the target area in the anterior corpus callosum (Bregma 1.1–0.8 mm), whose lateral boundaries are aligned with the inner edges of the lateral ventricles (shown in Fig. 1A, target area coloured in red, LV: lateral ventricle, CC: corpus callosum), and 2–3 coronal sections were selected to analyze cells in each mouse.

Sequential Immunohistochemistry

Sequential staining was performed according to the previous studies with minor modifications [15, 16]. Paraffin-embedded tissue sections were dewaxed with xylene and rehydrated through a series of graded alcohols to distilled water. Slides were stained with Mayer's hematoxylin, rinsed under running water, and then mounted in VectaMount AQ Aqueous Mounting Medium (Vector Laboratories; Burlingame, CA, USA, #H-5501). Whole-slide images were acquired using a slide scanner (see below), followed by rinsing with PBST (phosphate-buffered saline with 0.3% Triton-X100). For antigen retrieval, sections in a slide holder were transferred to a glass container filled with 1 L of the preheated retrieval solution (10 mM sodium citrate buffer, pH6.0; 95°C). The container was irradiated in a microwave oven and kept at the boiling temperature for 10 min, and then cooled to room temperature after which the slides were rinsed with PBST. Endogenous peroxidase was quenched in 3% hydrogen

peroxide for 10 min, followed by rinsing in PBST. Tissues were blocked in 10% normal donkey serum (Vector Laboratories) for 15 min to reduce non-specific staining, followed by incubation with primary antibody. Primary antibodies were incubated either overnight at 4°C or for 15 min in a microwave oven (MI-77, Azumaya, Tokyo, Japan) (for details of primary antibodies and incubation conditions, see Table S1). After washing with PBST, sections were incubated with secondary anti-mouse/anti-rabbit antibody (Histofine Simple Stain MAX PO; Nichirei Biosciences Inc., Tokyo, Japan) for 15 min at 37°C. After washing with PBST, peroxidase activity was revealed with AEC (Vector Laboratories). Slides were mounted in aqueous mounting medium and whole slide images were acquired. Cover glasses were removed, the slides were rinsed with PBST, and AEC staining was removed by immersion in ethanol. Antibodies were stripped by boiling tissue sections in pH 6 citrate buffer for 15 min. After rinsing with PBST, tissues were re-stained with different primary antibody, beginning with the blocking step described above. The following primary antibodies were applied in this order: NG2 (1:200, Abcam, rabbit); CC1 (1:50, Calbiochem, mouse); PDGFRα (1:200, Cell Signaling, rabbit); Olig1 (1:250, Millipore, mouse); Iba1 (1:200, Wako, rabbit); GFAP (1:600, Millipore, mouse); Ki67 (1:100, Abcam, rabbit). Primary antibodies were diluted in 1% normal donkey serum in PBST (Table S1). Controls for the validity of the multiplex staining were performed according to the previous study [16] and no cross-reaction was observed in our sequential staining steps (data not shown).

Microscopy and Image Analysis

For image analysis, digital whole-slide images of stained tissues were generated with a NanoZoomer 2.0-HT slide scanner (Hamamatsu Photonics, Hamamatsu, Japan) at 0.23 μm/pixel scanning resolution, and TIF images of tissue sections were obtained with NDP.view2 image viewing software (version 2.8.24, Hamamatsu Photonics). These images were overlaid as separate layers in Adobe Photoshop CS5 (Adobe Inc., San Jose, CA, USA). Hematoxylin-stained images were used as the background layer to determine the location of the cells.

Groups of cells that satisfied the following conditions were evaluated as LAs: containing three or more nuclei, being parallel to axonal orientation, and with the distance between each cell being less than 6.4 μm in paraffin sections with hematoxylin staining according to the definition set in a previous study [24]. In this definition, distance between nuclei of adjacent cells was less than a diameter of cellular nucleus. We randomly sampled thirty cells in a paraffin section of the corpus callosum and measured the diameters of the nuclei. The diameters ranged from 4.5 μm to 10.1 μm and the median was 6.4 μm. Accordingly, we set 6.4 μm as the representative diameter of cellular nucleus. The number of LAs and the number of cells in the LAs studied were as follows: young adult normal mice (n = 3) 299 arrays, 1400 cells; aged normal mice (n = 4) 410 arrays, 1692 cells; cuprizone model with four-week recovery period (+4w, n = 3) 391 arrays, 1477 cells; cuprizone model with 10-week recovery period (+10w, n = 4) 586 arrays, 2484 cells; cuprizone model with 24-week recovery period (+24w, n = 4) 500 arrays, 1997 cells. Cells separated from any other cells by more than 6.4 μm were analyzed as isolated cells (ICs). The numbers of analyzed ICs studied were as follows: young adult normal mice (n = 3) 673 cells; aged normal mice (n = 4) 1048 cells; cuprizone model with 24-week recovery period (+24w, n = 4) 1302 cells. All of the glial cells identified had either one of the staining patterns shown in the Fig.1D. When calculating the ratio of glial cells, the denominator was the total number of glial cells, and the each of the total ratio was 100% as shown in the Table S9.

Density of LAs and ICs

In a coronal section, an area of the corpus callosum between the lateral ventricles was acquired with ImageJ (version 1.53e) in young adult (n = 3, mean ± SEM = 0.74 ± 0.09 mm^2) and aged (n = 4, mean ± SEM = 0.72 ± 0.07 mm^2) mice. The density of LAs was calculated by dividing the sum of the number of LAs by the sum of the acquired areas (LAs/mm^2). The density of ICs was calculated by dividing the sum of the number of ICs by the sum of the acquired areas (cells/mm^2).

Density of Cells

Three boxed areas (x-axis, 0.20 mm and y-axis, 0.15 mm) were randomly selected in a corpus callosum section described above. Two sections were used for each mouse to obtain the density of cells (i.e., a total of six boxed areas were examined for each mouse). Hematoxylin staining was used to count the number of cells. The cell density was calculated by dividing the sum of the cell numbers by the sum of the area (6×0.20 mm $\times 0.15$ mm $= 0.18$ mm^2) (cells/0.18 mm^2). Young adult (n = 3) and aged (n = 4) normal mice, as well as mice at +1w (n = 3), +4w (n = 3), +10w (n = 4), and +24w (n = 4) of recovery period after cuprizone treatment, were used for the analysis.

Statistical Analysis

All statistical analyses were performed in R-studio (Version 1.3.1093, RStudio Team (2020). RStudio: Integrated Development for R. RStudio, PBC, Boston, MA, USA. URL http://www.rstudio.com/) with R (Version 4.0.3, R Core Team (2019). R: A language and environment for statistical computing. R Foundation for Statistical Computing, Vienna, Austria. URL https://www.R-project.org/). Student's t-tests were performed to compare two unpaired samples. For multiple comparisons, one-way analysis of variance (ANOVA) was applied with post-hoc Tukey honest significant difference (Tukey HSD) methods. $p < 0.05$ was considered statistically significant. Asterisks indicate significant differences (* $p < 0.05$, ** $p < 0.01$, *** $p < 0.001$). Dagger indicates significant tendency († $p = 0.05$).

Results

Cell Alignment and Formation of LAs Appear in Accordance with Myelination in the Postnatal Corpus Callosum

We first examined cellular distribution and myelination patterns in the developing corpus callosum (Fig. 1A). At P7, cellular nuclei stained for DAPI were dispersed, with random distances between them. We observed few MBP-immunoreactive structures at this stage. The distribution pattern of the nuclei

changed significantly at P14: the cells became close to each other and formed LAs reminiscent of pearls-on-a-string. Concurrent with this change, MBP-positive myelin sheaths became more abundant and appeared as distinct fibers. In the 8-week-old mouse (young adult), the cellular arrays became dominant, with more cells in each array compared to arrays at P14. Mature myelinated fibers exhibited thick and dense MBP staining. These developmental changes imply that cellular array formation plays roles in myelination of axons and/or maintenance of myelin sheaths.

Definition of the LAs and the ICs in the Adult Corpus Callosum

To characterize the cellular composition of the corpus callosum, we next defined a LA as a group of three or more cells aligned in a straight line (Fig. 1B, red arrowheads in the hematoxylin-stained corpus callosum at 8 weeks of age). The single cells distant from LAs were defined as ICs whose nuclei were more than 6.4 μm from others (Fig. 1B, blue arrowheads). These definitions are based on the cellular distribution in paraffin sections (2 μm thick). It should be noted that the numbers of ICs may be overestimated because a single IC may have had adjacent cell(s) in the neighboring paraffin sections, making a LA mistakenly recognized as an IC. Conversely, the number of LAs may be underestimated.

Multiplex Staining Reveals Glial Heterogeneity in the Corpus Callosum of 8-Week-Old Young Adult Mice

Fig. 1C shows representative images of a LA labeled by the multiplex staining method. The left-most column illustrates a LA with six adjacent cells (numbered 1–6) stained with hematoxylin. Other columns display immunoreactions of markers, with the immunostaining sequence shown from left to right (i.e., starting from NG2 and ending in Ki67 labeling). The marker staining pattern of No. 1, 3, and 5 cells (CC1+, Olig1+, NG2−, PDGFRα−) was most abundant (more than 80% of total cells) in the corpus callosum, indicating that these cells were mature myelinating oligodendrocytes (see also Fig. 1D (5)). Other oligodendrocyte lineage cells were defined as immature oligodendrocytes, and

according to a previous literature [14], we further classified the immature oligodendrocytes into oligodendrocyte progenitor cells (OPCs) and premyelinating oligodendrocytes with a battery of developmental markers. OPCs were positive for Ki67 and/or PDFGRα in addition to other oligodendrocyte lineage markers (Fig. 1D (1) and (2)). The immature oligodendrocytes lost expression of the two proteins (Ki67 and PDGFRα), but had other markers (NG2, Olig1, and CC1) were regarded as premyelinating oligodendrocytes. The No. 2 cell in the Fig. 1C (CC1−, Olig1+, NG2−, PDGFRα−) was a representative premyelinating oligodendrocyte (see also Fig. 1D (3) and (4)). The No. 4 cell was positive only for Iba1 and considered to be microglia (see also Fig. 1D (7)). The No. 6 cell was a GFAP+ astrocyte (see also Fig. 1D (6)). The representative LA consisted of a heterogeneous glial population, confirming the glial heterogeneity in the corpus callosum. Given this result, we checked all the LAs identified in the present study to determine whether they are composed of homogeneous mature oligodendrocytes or of heterogeneous glial species like the representative LA (Fig. 1C). 46.72 ± 1.72% (all statistical data are hereafter expressed as mean ± SEM) of the LAs were homogeneous and the remaining 53.28 ± 1.72% contained at least one astrocyte, microglia, or immature oligodendrocyte in addition to mature oligodendrocytes. 23.41 ± 0.97% of LAs contained more than one astrocyte, 19.60 ± 1.74% of LAs contained more than one microglia, and 25.30 ± 1.88% of LAs contained more than one immature oligodendrocyte.

Characterization of Cells in the Corpus Callosum of 8-Week-Old Young Adult Mice

Consistent with previous studies, the corpus callosum of the young adult mouse contains immature OLs; significantly more immature OLs existed in the ICs than in the LAs (Fig. 2A; LAs: 6.48 ± 0.62%, ICs: 10.04 ± 0.47%, $p < 0.05$). Further classification revealed that OPCs were the main cause of the difference in distribution patterns (Fig. 2B; LAs: 2.78 ± 0.37%, ICs: 5.03 ± 0.44%, $p < 0.05$), while the premyelinating OLs were comparable between two cellular populations (Fig. 2C; LAs: 3.70 ± 0.65%, ICs: 5.01 ± 0.53%). We confirmed that the majority of the cells in the corpus callosum were

mature myelinating oligodendrocytes (Olig1+, CC1+, PDGFRα−, NG2−) (Fig. 2D; LAs: 83.60 ± 0.38%, ICs: 84.36 ± 1.15%). Astrocytes were also observed at equal levels in both LAs and ICs (Fig. 2E; LAs: 5.58 ± 0.43%, ICs: 4.19 ± 0.83%). Interestingly, microglia were more abundant in the LAs (Fig. 2F; LAs: 4.34 ± 0.59%, ICs: 1.41 ± 0.18%, $p < 0.01$). Based on these results, LAs did not form merely by chance, implying some meanings in the locational polarity of these cells and the formation of LAs.

Microglia of Aged Mice Also Have Polarized Distribution in the Corpus Callosum

Next, we asked if 32-week-old aged mice also have a similar cell distribution to those in the young adult mice. The labeling patterns of LAs and ICs in the aged mice were almost identical to those in the young adult mice. Immature OLs no longer showed polarized distribution (Fig. 3A; LAs: 5.17 ± 0.70%, ICs: 7.44 ± 1.28%). When we analyzed OPCs (Fig. 3B; LAs: 3.78 ± 0.73%, ICs: 5.29 ± 0.84%) or premyelinating OLs (Fig. 3C; LAs: 1.40 ± 0.20%, ICs: 2.15 ± 0.48%), no significant difference was found. Mature OLs (Fig. 3D; LAs: 84.77 ± 0.17%, ICs: 85.80 ± 1.22%) and astrocytes (Fig. 3E; LAs: 5.85 ± 0.70%, ICs: 4.78 ± 0.53%) displayed similar ratios regardless of the location of the cells, while microglia showed a preference for localization in the LAs (Fig. 3F; LAs: 4.20 ± 0.52%, ICs: 1.98 ± 0.60%, $p < 0.05$), which corresponded with the results for young adult mice (Fig. 2F). These observations suggest that the polarity of distribution between LAs and ICs is lost during aging for most glial components, except for microglia.

Premyelinating OLs and Number of Cells per LA Decrease with Aging

Based on the idea that aging affects glial cell localization, we next focused specifically on the LAs and compared the glial compositions in young adult and aged mice. The ratios of immature OLs (Fig. 4A; young adult: 6.48 ± 0.62%, aged: 5.17 ± 0.70%) and OPCs (Fig. 4B; young adult: 2.78 ± 0.37%, aged: 3.78 ± 0.73%) were comparable between the two groups. The premyelinating OLs, however, showed

an apparent decrease in the ratio during aging (Fig. 4C; young adult: 3.70 ± 0.65%, aged: 1.40 ± 0.20%, $p < 0.05$). The ratio of mature OLs in the aged mice was slightly but significantly higher than that in young adult mice (Fig. 4D; young adult: 83.60 ± 0.38%, aged: 84.77 ± 0.17%, $p < 0.05$). The ratios of astrocytes (Fig. 4E; young adult: 5.58 ± 0.43%, aged: 5.85 ± 0.70%) and microglia (Fig. 4F; young adult: 4.34 ± 0.59%, aged: 4.20 ± 0.52%) did not change significantly with aging. Premyelinating OLs in the young mice may mature with age and this process could result in a decrease of premyelinating OLs and an increase of mature OLs in the aged mice. Interestingly, the cell numbers in each LA became significantly smaller as the mice aged (Fig. 4G; young adult: 4.68 ± 0.07, aged: 4.11 ± 0.15, $p < 0.05$), which may conflict with the above-described cellular maturation. Possible explanations for the discrepancy are that some of the premyelinating OLs, during their maturation, either die or dissociate from LAs. Density analyses of LAs (Fig. 4H; young adult: 135.67 ± 6.16 cells/mm^2, aged: 143.16 ± 12.82 cells/mm^2) and ICs (Fig. 4I; young adult: 302.74 ± 16.99 cells/mm^2, aged: 366.65 ± 11.92 cells/mm^2, $p < 0.05$) in the young adult and aged mice favor the latter possibility: the density of ICs was significantly higher in aged mice than in young adult mice (Fig. 4I). This evidence is indirect, however, and further lineage tracing experiments will be needed to test the hypothesis.

We also compared the ratio of glial populations in ICs between young adult and aged mice (Fig. S1A-F). The premyelinating OLs in the ICs were significantly decreased by aging but there was no significant difference between the mature OLs in ICs.

LAs Re-form in the Corpus Callosum When Remyelination Progresses in the Adult Cuprizone Mouse Model

To further clarify the relationship between the formation of LAs and myelination, we used the cuprizone mouse model. Cuprizone induces toxic demyelination, and its withdrawal induces spontaneous remyelination. Cuprizone was administered to 8-week-old mice for 4 weeks, after which the mice were put on a normal chow to induce remyelination. Mice were sacrificed after 1, 4, 10, and

24 weeks of recovery (+1w, +4w, +10w, and +24w). Control mice were fed normal chow without cuprizone.

To determine the time course of cuprizone-induced demyelination and remyelination, myelin was analyzed by immunohistochemistry (Fig. 5A, upper panels). MBP immunoreactivity revealed an almost complete demyelination of the corpus callosum in +1w mice. Significant remyelination was observed in the mice at +4w, +10w, and +24w. Nuclei were stained deep blue with hematoxylin (Fig. 5A, middle and lower panels). Unlike in healthy young (8 weeks) and aged (32 weeks) adult mice, LAs were no longer observed and cells in the corpus callosum were located randomly at 1 week after cuprizone treatment (+1w). LAs were gradually restored in the +4w, +10w, and +24w mice. The re-formation of LAs appeared concurrent with the extent of remyelination, recapitulating the postnatal development of the corpus callosum (Fig. 1A). This result supports the theory that creation of LAs plays an important role in the formation and maintenance of the myelin sheath.

We also examined cell density (all cells in a field were counted) (Fig. 5B). Shared letters above the boxplots mark significantly different pairs ($p < 0.001$). Cell density was greatly increased at +1w (905.00 ± 16.04) compared to young adult control mice (310.33 ± 11.05). It declined slightly at +4w (572.33 ± 44.67) but never came down to the level of the control mice even at +24w (535.00 ± 31.02). No significant difference was found between young adult and aged (316.00 ± 15.96) control mice.

Time Course of the Ratio of Glial Cells in LAs After Cuprizone Treatment

The ratio of immature OLs significantly decreased from +10w to +24w (Fig. 5C; +4w: 7.28 ± 0.88%, +10w: 8.98 ± 0.64%, +24w: 6.15 ± 0.24%, $p < 0.05$ between +10w and +24w). Consistent with the previous results, the ratio of OPCs was stable, with no significant differences between demyelinated or remyelinated stages (Fig. 5D; +4w: 3.26 ± 0.34%, +10w: 2.80 ± 0.34%, +24w: 3.12 ± 0.69%). The ratio of premyelinating OLs changed in accordance with the ratio of immature OLs in the LAs during the remyelination process (Fig. 5E; +4w: 4.02 ± 0.78%, +10w: 6.18 ± 0.35%, +24w: 3.03 ± 0.49%, p

= 0.05 between +4w and +10w, $p < 0.01$ between +10w and +24w). The mature OL ratios gradually increased from +4w until +24w (Fig. 5F; +4w: 61.42 ± 1.61%, +10w: 68.88 ± 1.12%, +24w: 76.08 ± 1.73%, $p < 0.05$ between +4w and +10w, $p < 0.001$ between +4w and +24w, $p < 0.05$ between +10w and +24w). Astrocytes showed no significant change throughout the examination period (Fig. 5G; +4w: 13.25 ± 0.66%, +10w: 15.46 ± 1.08%, +24w: 13.49 ± 1.78%). Microglia became less abundant in the LAs (Fig. 5H; +4w: 18.05 ± 2.82%, +10w: 6.68 ± 0.95%, +24w: 4.28 ± 0.21%, $p < 0.01$ between +4w and +10w, $p < 0.001$ between +4w and +24w). Interestingly, even though the ratio of microglia in the LAs decreased significantly from +4w to +10w, the average number of cells in a single LA increased (Fig. 5I; +4w: 3.77 ± 0.08 cells/LA, +10w: 4.23 ± 0.09 cells/LA, +24w: 4.02 ± 0.09 cells/LA, $p < 0.05$ between +4w and +10w). Premyelinating OLs and mature OLs seem to augment the number of cells in the LAs, compensating for the loss of microglia (Fig. 5I).

Microglia Display Polarized Distribution in the Remyelinated Corpus Callosum at +24w

We next focused on the glial populations at +24w, when remyelination after cuprizone treatment is completed [21, 25]. The ratio of immature OLs showed no difference between LAs and ICs (Fig. 6A; LAs: 6.15 ± 0.24%, ICs: 5.65 ± 0.39%). Moreover, the ratios of OPCs (Fig. 6B; LAs: 3.12 ± 0.69%, ICs: 1.56 ± 0.28%) and premyelinating OLs (Fig. 6C; LAs: 3.03 ± 0.49%, ICs: 4.09 ± 0.33%) also showed no significant difference between LAs and ICs. These levels are comparable to those in aged control mice (Fig. 3). The ratios of the mature OLs (Fig. 6D; LAs: 76.08 ± 1.73%, ICs: 77.51 ± 1.49%) and astrocytes (Fig. 6E; LAs: 13.49 ± 1.78%, ICs: 14.76 ± 1.96%) were also similar between LAs and ICs. However, when we compared the mean values of the ratios between +24w and aged control (Fig. 3D and E), the mature OLs were decreased and in turn astrocytes were increased in the +24w corpus callosum regardless of the cellular location. The polarity of microglial distribution was regained in the +24w mice (Fig. 6F; LAs: 4.28 ± 0.21%, ICs: 2.09 ± 0.75%, $p < 0.05$), recapitulating the microglial bias toward the LAs in the aged control mice.

Discussion

The corpus callosum continues to develop in humans and other animals until adolescence [2, 13, 26–29]. Consistent with this, we found that OPCs were abundant in the ICs in eight-week-old mice (Fig. 2B). Since OPCs are known to self-renew very slowly during postnatal development [29, 30], ICs that are OPCs may generate LAs during the aging process. In this regard, it is noteworthy that premyelinating OLs are more abundant in the young adult LAs than in the aged LAs (Fig. 4C). These findings suggest that the corpus callosum of the young adult is still undergoing maturation.

Our finding that the LAs contain more microglia than the ICs suggests that the microglia play a role in the formation and/or maintenance of LAs. The biased localization of microglia to LAs in the 32-week-old corpus callosum supports this hypothesis. Even after demyelination–remyelination processes, microglia were significantly more abundant in the LAs than in the ICs (Fig. 6F and S2). In the developing white matter, microglia promote myelination [6, 8, 31–33], and remyelination in the adult brain is also enhanced by microglia [34–37]. Cooperation between microglia and astrocytes also plays important roles in the adult corpus callosum, especially in pathological conditions. For example, microglia support remyelination in the CNS after injury via phagocytic removal of remyelination-inhibiting myelin debris and by secreting growth factors for OPC proliferation and differentiation [30, 36], and astrocytes recruit and initiate microglia to clear this debris [37]. It is possible that the microglia in the LAs are involved in the myelination and remyelination, but the aged corpus callosum probably does not undergo myelin remodeling. Recent RNA sequencing analyses have uncovered the heterogeneity of the microglia in adult and aged white matter [38–40]. The subset of microglia called white matter-associated microglia plays important roles in white matter degeneration [39]. It would be of particular interest to examine the molecular signatures of microglia in the LAs and the ICs. Specific depletion of microglia could be another interesting approach to elucidating the functional implications of microglia in the LAs. The linear distribution of cells may become disarranged if the microglia in

the LAs exert homeostatic functions in white matter morphology. Recent work has partially uncovered the complex interactions of glial cells in the white matter. For example, astrocytes provide lipids for producing the myelin sheath [4], and extracellular vesicles from astrocytes support oligodendrocyte differentiation [5]. A single mutation in astrocytic GFAP (glial fibrillary acidic protein) causes OPC and oligodendrocyte loss and demyelination [41–43]. The present study revealed that the numbers of astrocytes in the corpus callosum are kept high after demyelination–remyelination processes (Fig. 5G). Twenty-four weeks are long enough for the astrocytes to become non-reactive. Unlike the microglia, these astrocytes were distributed both in the LAs and the ICs (Fig. 6E). It is possible that the astrocytes form a framework for axonal tracts [18]. Visualization of fine processes with genetic marking [44] may answer this question and is under investigation.

Acknowledgements

We thank Prof. Hiroki Kuniyasu (Department of Molecular Pathology, Nara Medical University) for enabling us to use NanoZoomer scanner. We thank Mr. Koji Okuda for his technical assistance in making paraffin sections. We also thank Dr. Ian Smith (Elite Scientific Editing) for his thorough editing of our manuscript.

Author Contribution

YK and KT conceived and designed the experiments; YK, AI, TT, KN, and KT performed the experiments. YK, KT, and AW analyzed and interpreted the results of the experiments. YK, KT, and AW wrote the manuscript. All authors have read and approved the manuscript.

Funding

This work was supported by JSPS KAKENHI JP19K06928 (to KT), JP19K07827 (to TT), JP19K16480 (to AI), JP21K06758 (to AW), the Osaka Medical Research Foundation for Intractable

Diseases (to TT), the Takeda Science Foundation (to TT), the Nakatomi Foundation (to TT), the Naito Foundation (to TT), and the Ichiro Kanehara Foundation (to TT).

Declarations

Data availability All data generated or analysed in this study are included in this published article [and its supplementary information files].

Conflict of interest The authors declare that they have no competing interests.

References

1. Roland JL, Snyder AZ, Hacker CD, et al (2017) On the role of the corpus callosum in interhemispheric functional connectivity in humans. Proc Natl Acad Sci U S A 114:13278–13283

2. Vannucci RC, Barron TF, Vannucci SJ (2017) Development of the Corpus Callosum: An MRI Study. Dev Neurosci 39:97–106

3. Pujol J, Vendrell P, Junqué C, et al (1993) When does human brain development end? Evidence of corpus callosum growth up to adulthood. Ann Neurol 34:71–75

4. Camargo N, Goudriaan A, van Deijk A-LF, et al (2017) Oligodendroglial myelination requires astrocyte-derived lipids. PLoS Biol 15:e1002605

5. Willis CM, Nicaise AM, Bongarzone ER, et al (2020) Astrocyte Support for Oligodendrocyte Differentiation can be Conveyed via Extracellular Vesicles but Diminishes with Age. Sci Rep 10:828

6. Traiffort E, Kassoussi A, Zahaf A, Laouarem Y (2020) Astrocytes and Microglia as Major Players of Myelin Production in Normal and Pathological Conditions. Front Cell Neurosci 14:79

7. Domingues HS, Portugal CC, Socodato R, Relvas JB (2016) Oligodendrocyte, Astrocyte, and Microglia Crosstalk in Myelin Development, Damage, and Repair. Front Cell Dev Biol 4:71

8. Wlodarczyk A, Holtman IR, Krueger M, et al (2017) A novel microglial subset plays a key role in myelinogenesis in developing brain. EMBO J 36:3292–3308

9. Hagemeyer N, Hanft K-M, Akriditou M-A, et al (2017) Microglia contribute to normal

myelinogenesis and to oligodendrocyte progenitor maintenance during adulthood. Acta Neuropathol 134:441–458

10. Barber HM, Ali MF, Kucenas S (2022) Glial Patchwork: Oligodendrocyte Progenitor Cells and Astrocytes Blanket the Central Nervous System. Front Cell Neurosci 15:536

11. Huang W, Bhaduri A, Velmeshev D, et al (2020) Origins and Proliferative States of Human Oligodendrocyte Precursor Cells. Cell. https://doi.org/10.1016/j.cell.2020.06.027

12. Tatsumi K, Haga S, Matsuyoshi H, et al (2005) Characterization of cells with proliferative activity after a brain injury. Neurochem Int 46:381–389

13. Chong SYC, Chan JR (2010) Tapping into the glial reservoir: cells committed to remaining uncommitted. J Cell Biol 188:305–312

14. Nishiyama A, Komitova M, Suzuki R, Zhu X (2009) Polydendrocytes (NG2 cells): multifunctional cells with lineage plasticity. Nat Rev Neurosci 10:9–22

15. Glass G, Papin JA, Mandell JW (2009) SIMPLE: a sequential immunoperoxidase labeling and erasing method. J Histochem Cytochem 57:899–905

16. Tsujikawa T, Kumar S, Borkar RN, et al (2017) Quantitative Multiplex Immunohistochemistry Reveals Myeloid-Inflamed Tumor-Immune Complexity Associated with Poor Prognosis. Cell Rep 19:203–217

17. Kahn S, Tansey FA, Cammer W (1986) Biochemical and immunocytochemical evidence for a deficiency of normal interfascicular oligodendroglia in the CNS of the dysmyelinating mutant (md) rat. J Neurochem 47:1061–1065

18. Suzuki M, Raisman G (1992) The glial framework of central white matter tracts: segmented rows of contiguous interfascicular oligodendrocytes and solitary astrocytes give rise to a continuous meshwork of transverse and longitudinal processes in the adult rat fimbria. Glia 6:222–235

19. Tanaka T, Ohno N, Osanai Y, et al (2021) Large-scale electron microscopic volume imaging of interfascicular oligodendrocytes in the mouse corpus callosum. Glia. https://doi.org/10.1002/glia.24055

20. Carlton WW (1967) Studies on the induction of hydrocephalus and spongy degeneration by cuprizone feeding and attempts to antidote the toxicity. Life Sci 6:11–19

21. Steelman AJ, Thompson JP, Li J (2012) Demyelination and remyelination in anatomically distinct regions of the corpus callosum following cuprizone intoxication. Neurosci Res 72:32–42

22. Islam MS, Tatsumi K, Okuda H, et al (2009) Olig2-expressing progenitor cells preferentially differentiate into oligodendrocytes in cuprizone-induced demyelinated lesions. Neurochem Int 54:192–198

23. Gudi V, Moharregh-Khiabani D, Skripuletz T, et al (2009) Regional differences between grey and white matter in cuprizone induced demyelination. Brain Res 1283:127–138

24. Walsh DM, Röth PT, Holmes WR, et al (2016) Is cell migration or proliferation dominant in the formation of linear arrays of oligodendrocytes? J Theor Biol 406:17–30

25. Skripuletz T, Gudi V, Hackstette D, Stangel M (2011) De- and remyelination in the CNS white and grey matter induced by cuprizone: the old, the new, and the unexpected. Histol Histopathol 26:1585–1597

26. Goddings A-L, Roalf D, Lebel C, Tamnes CK (2021) Development of white matter microstructure and executive functions during childhood and adolescence: a review of diffusion MRI studies. Dev Cogn Neurosci 51:101008

27. Pagnin M, Kondos-Devcic D, Chincarini G, et al (2021) Role of thyroid hormones in normal and abnormal central nervous system myelination in humans and rodents. Front Neuroendocrinol 61:100901

28. Ku RY, Torii M (2020) New Molecular Players in the Development of Callosal Projections. Cells 10:. https://doi.org/10.3390/cells10010029

29. Marques S, Zeisel A, Codeluppi S, et al (2016) Oligodendrocyte heterogeneity in the mouse juvenile and adult central nervous system. Science 352:1326–1329

30. Clarke LE, Young KM, Hamilton NB, et al (2012) Properties and fate of oligodendrocyte progenitor cells in the corpus callosum, motor cortex, and piriform cortex of the mouse. J Neurosci 32:8173–8185

31. Irfan M, Evonuk KS, DeSilva TM (2021) Microglia phagocytose oligodendrocyte progenitor cells and synapses during early postnatal development: implications for white versus gray matter maturation. FEBS J. https://doi.org/10.1111/febs.16190

32. Santos EN, Fields RD (2021) Regulation of myelination by microglia. Sci Adv 7:eabk1131

33. Kalafatakis I, Karagogeos D (2021) Oligodendrocytes and Microglia: Key Players in Myelin Development, Damage and Repair. Biomolecules 11:. https://doi.org/10.3390/biom11071058

34. Miron VE, Boyd A, Zhao J-W, et al (2013) M2 microglia and macrophages drive oligodendrocyte

differentiation during CNS remyelination. Nat Neurosci 16:1211–1218

35. Rawji KS, Mishra MK, Yong VW (2016) Regenerative Capacity of Macrophages for Remyelination. Front Cell Dev Biol 4:47

36. Lloyd AF, Miron VE (2019) The pro-remyelination properties of microglia in the central nervous system. Nat Rev Neurol 15:447–458

37. Karamita M, Barnum C, Möbius W, et al (2017) Therapeutic inhibition of soluble brain TNF promotes remyelination by increasing myelin phagocytosis by microglia. JCI Insight 2:. https://doi.org/10.1172/jci.insight.87455

38. Amor S, McNamara NB, Gerrits E, et al (2022) White matter microglia heterogeneity in the CNS. Acta Neuropathol 143:125–141

39. Safaiyan S, Besson-Girard S, Kaya T, et al (2021) White matter aging drives microglial diversity. Neuron 109:1100-1117.e10

40. Hanisch U-K (2013) Functional diversity of microglia - how heterogeneous are they to begin with? Front Cell Neurosci 7:65

41. Brenner M, Johnson AB, Boespflug-Tanguy O, et al (2001) Mutations in GFAP, encoding glial fibrillary acidic protein, are associated with Alexander disease. Nat Genet 27:117–120

42. Prust M, Wang J, Morizono H, et al (2011) GFAP mutations, age at onset, and clinical subtypes in Alexander disease. Neurology 77:1287–1294

43. Li L, Tian E, Chen X, et al (2018) GFAP Mutations in Astrocytes Impair Oligodendrocyte Progenitor Proliferation and Myelination in an hiPSC Model of Alexander Disease. Cell Stem Cell 23:239-251.e6

44. Tatsumi K, Isonishi A, Yamasaki M, et al (2018) Olig2-Lineage astrocytes: A distinct subtype of astrocytes that differs from GFAP astrocytes. Front Neuroanat 12:8

Legend for Figures

Fig. 1 A: Cell nuclei (stained with DAPI; white) and myelin basic protein (MBP) immunostaining (green fluorescence) during postnatal development (P7: 7 days old; P14: 14 days old; young adult: 8 weeks old). B: Hematoxylin-stained image of the corpus callosum at 8 weeks of age. Cell nuclei are stained dark blue. Red arrowheads indicate cell nuclei forming a LA, and blue arrowheads indicate IC nuclei. C: Representative example of multiplex staining in the 8-week-old corpus callosum, showing a single LA consisting of six cells (numbered 1–6), starting with hematoxylin on the leftmost side and moving rightward to NG2, CC1, PDGFRα, Olig1, Iba1, GFAP and Ki67. D: Expression patterns of the seven cell markers listed in C, with cell types deduced from labeling combinations shown in the left table. MG: microglia; AS: astrocyte; OLs: oligodendrocytes. Oligodendrocyte lineage cells were classified as mature (M-OLs) and premyelinating OLs (PM-OLs), and oligodendrocyte progenitor cells (OPCs). Numbers in brackets in the table correspond to those in the representative cell images on the right; other cells (not shown) displayed other marker combinations that also identified them as OPCs or PM-OLs, as indicated by the non-numbered entries in the table. Positive reactions are highlighted with thick-bordered squares.

Fig. 2 Cells belonging to LAs (299 arrays, 1400 cells) and ICs (673 cells) were identified in the corpus callosum of 8-week-old young adults (n = 3). Comparison between immature OLs (OPCs+ premyelinating OLs) in LAs and those in ICs is shown (A), followed by comparisons of OPCs (B), premyelinating OLs (C), mature OLs (D), astrocytes (E), and microglia (F). Statistically significant differences are indicated by * ($p < 0.05$) and ** ($p < 0.01$). For all the statistical data, see Table S2 (Supplement).

Fig. 3 LAs (410 arrays, 1692 cells) and ICs (1048 cells) cell populations were identified in the corpus

callosum of 32-week-old aged mice (n = 4) as in Fig. 2, and the percentage of each cell type was compared in each population. A: Immature OLs, B: OPCs, C: Premyelinating OLs, D: Mature OLs, E: Astrocytes, F: Microglia. (* indicates $p < 0.05$). All the statistical data are shown in the Table S3.

Fig. 4 We compared the percentages of cell populations in LAs between young adult and aged mice (A–F, as in Fig. 2), the number of cells in a single LA (G), the number of LAs (H) in the target area, and the number of ICs (I) in the target area (see Tissue Preparation in Materials and Methods) between young adult (n = 3) and aged mice (n = 4) (* indicates $p < 0.05$). All the statistical data are shown in the Table S4.

Fig. 5 A: Top panel: MBP immunostaining (gray scale). Middle panel: low magnification views of cell nuclei (blue) stained with hematoxylin. Bottom panel: higher-magnification views of cell nuclei. From left to right: young adult, 1 week, 4 weeks, 10 weeks, 24 weeks after completion of cuprizone administration, and aged corpus callosum (the borders of the corpus callosum are indicated by dashed lines in low-magnification views). B: Cell density was compared in young adult, 1w, 4w, 10w, 24w after cuprizone treatment, and aged corpus callosum. Data from 3–4 brains (n = 3 for young adult, +1w, and +4w, n = 4 for +10w, +24w, and aged) were used to label pairs with a–k if there was a significant difference ($p < 0.001$) between them. All the statistical data in Fig. 5B are shown in the Table S6. C: Percentage of immature OLs present in the LAs at 4 weeks (+4w), 10 weeks (+10w), and 24 weeks (+24w) after cuprizone treatment. There was a significant decrease in immature OLs at 24 weeks compared to 10 weeks. D: Comparing OPCs as in C, there was no significant difference between any time. E: Comparing premyelinating OLs, there was a significant tendency of increase at 10 weeks compared with 4 weeks and a significant decrease at 24 weeks from 10 weeks. F: Mature OLs increased significantly at 4 weeks, 10 weeks, and 24 weeks. G: Astrocytes did not show any significant change between any two periods. H: Microglia were abundant at 4 weeks and decreased significantly at 10

and 24 weeks. I: The number of cells in a single LA was low at 4 weeks and significantly increased at 10 weeks. († $p = 0.05$, * $p < 0.05$, ** $p < 0.01$, *** $p < 0.001$) All the statistical data of Fig. 5C-I are shown in the Table S7.

Fig. 6 Percentages of various cell types in the LA and IC populations at 24 weeks after completion of cuprizone treatment. No significant difference was observed in immature OLs (A), OPCs (B), premyelinating OLs (C), mature OLs (D), or astrocytes (E). Microglia (F) were significantly (* $p < 0.05$) more abundant in LAs than in ICs. All the statistical data are shown in the Table S8.

Figure 1

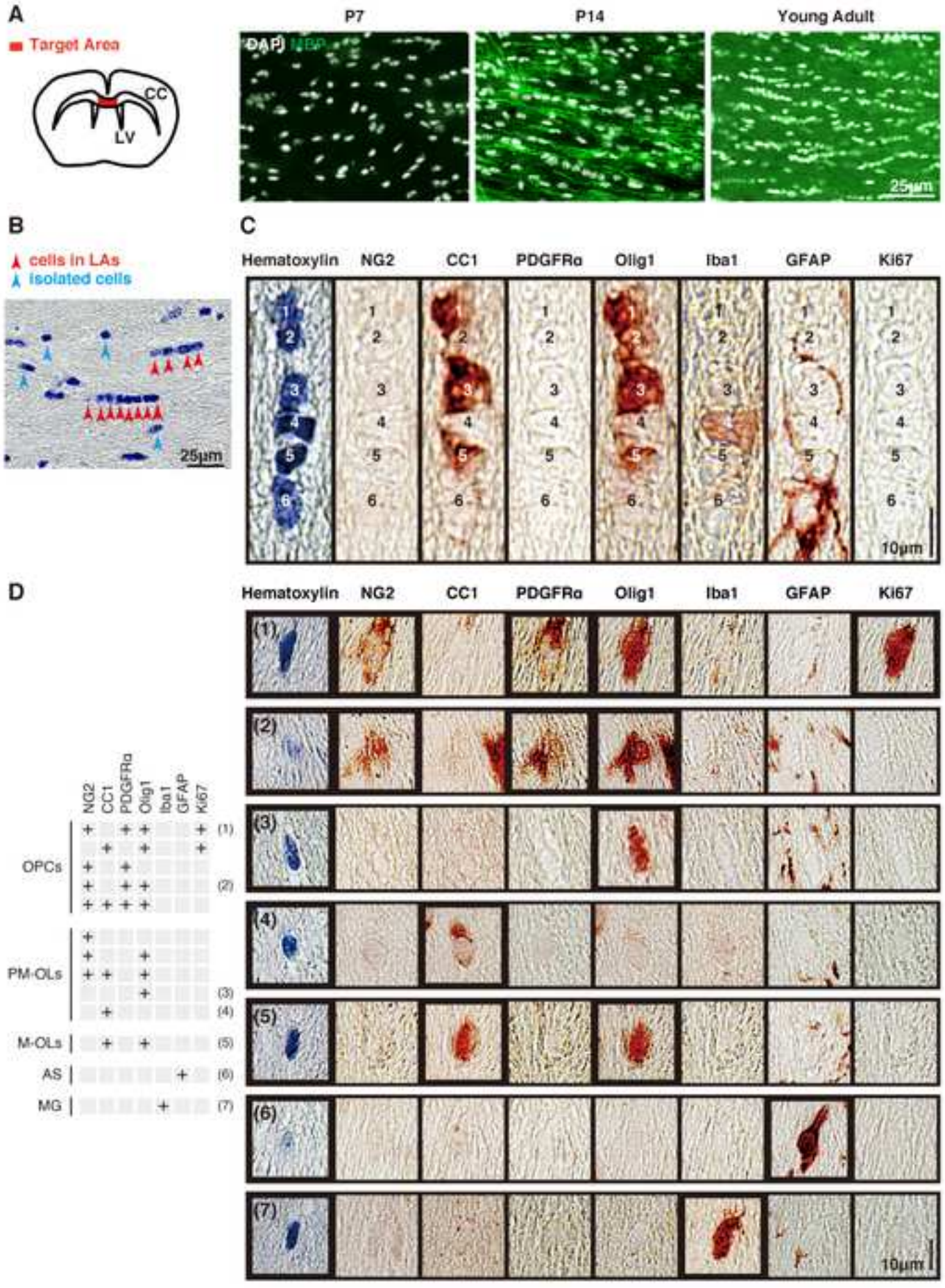

Figure 2

Click here to access/download;Figure;FIGURE 2.pdf

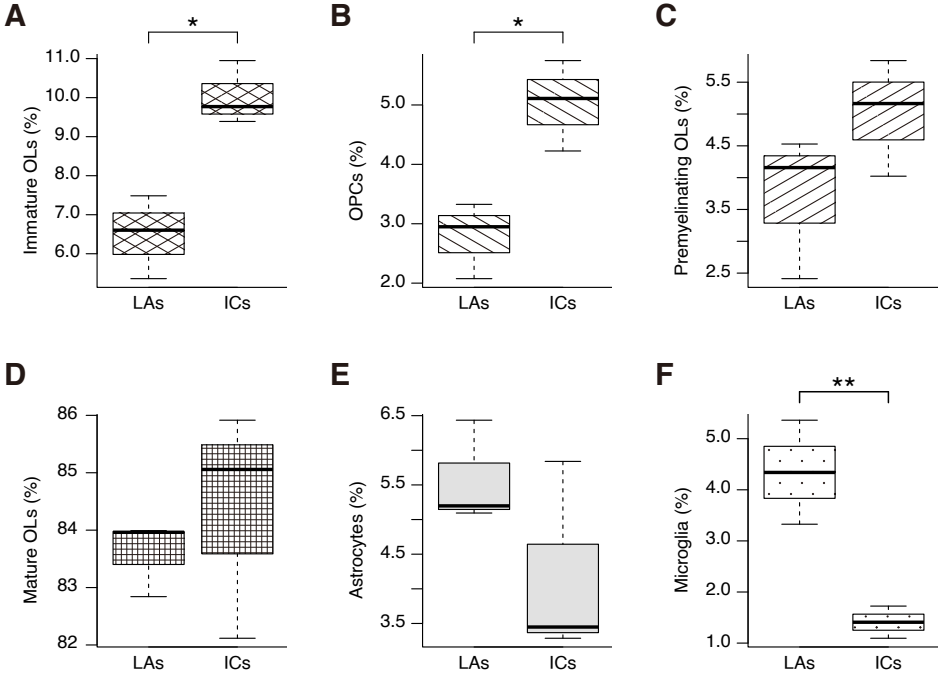

Figure 3

Click here to access/download;Figure;FIGURE 3.pdf

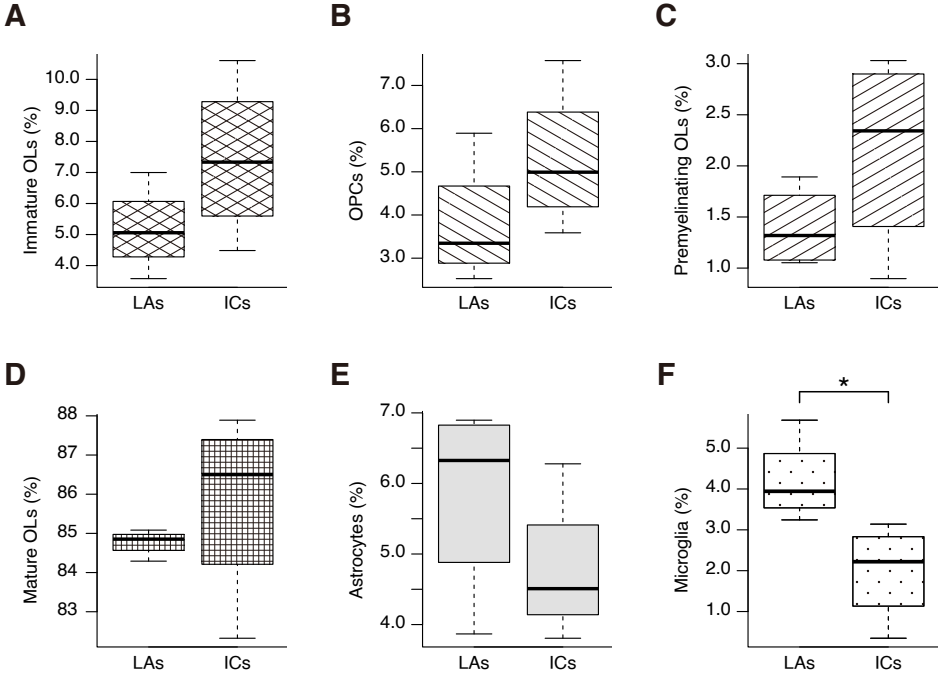

Figure 4

Click here to access/download;Figure;FIGURE 4.pdf

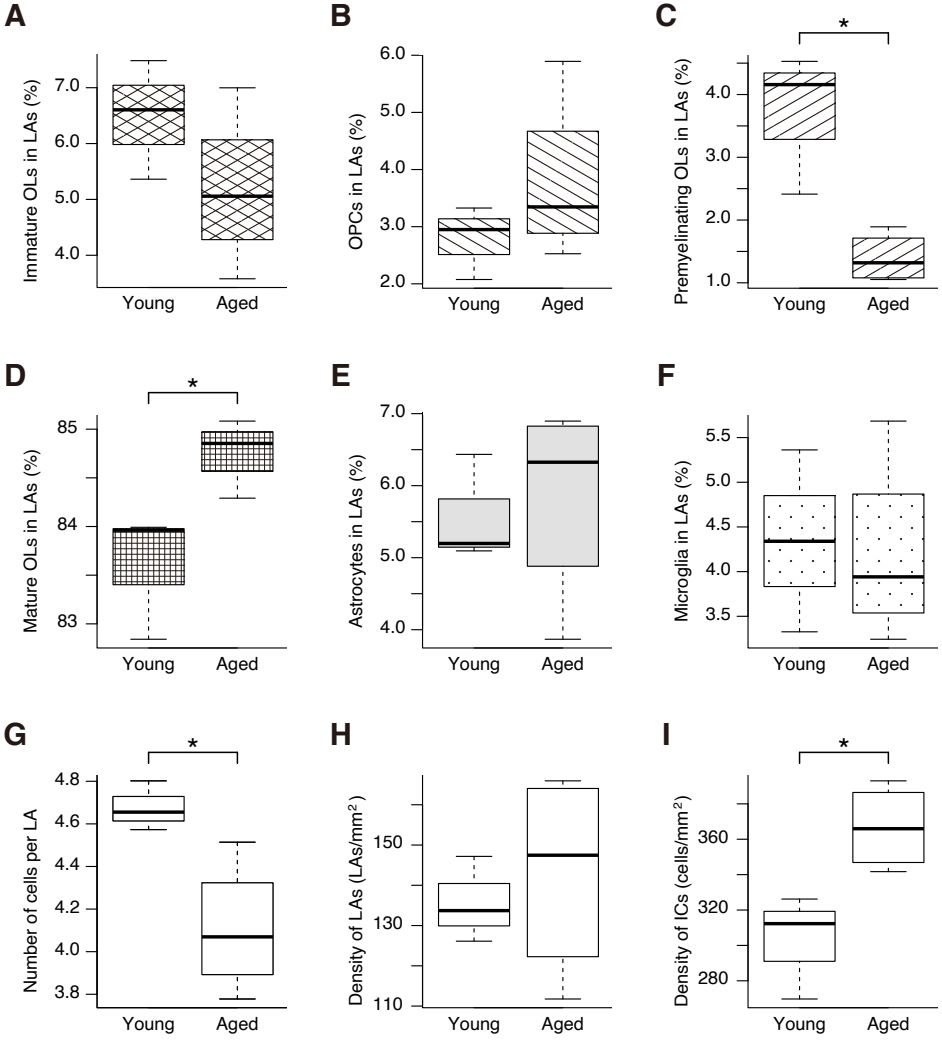

Figure 5

Click here to access/download;Figure;figure5 small1.pdf

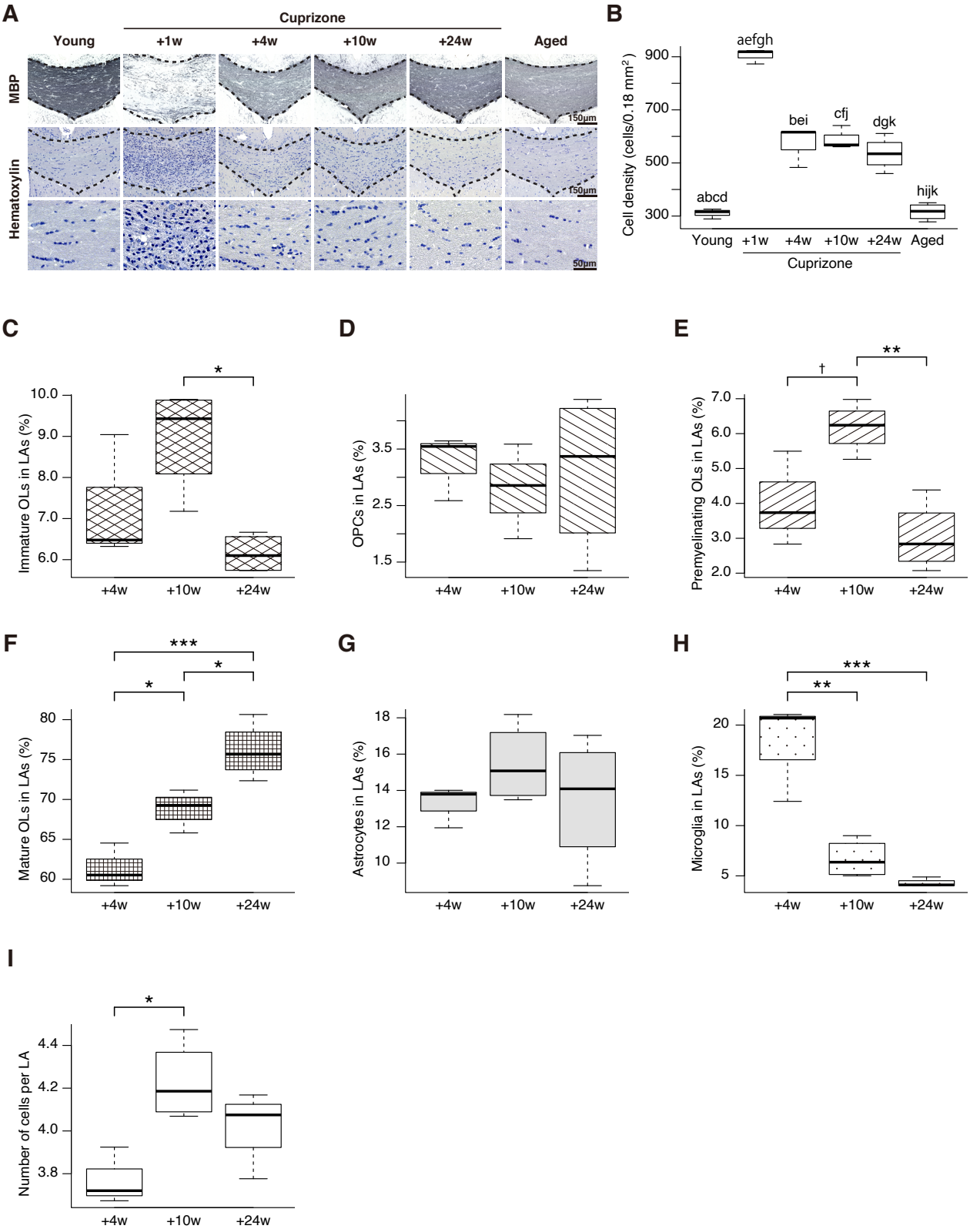

Figure 6

Click here to access/download;Figure;FIGURE 6.pdf